
Article:
Pessu, F orcid.org/0000-0003-3587-4309, Barker, RJ orcid.org/0000-0002-5106-6929 and Neville, A orcid.org/0000-0002-6479-1871 (2015) The Influence of pH on localized corrosion behavior of X65 Carbon Steel in CO2-Saturated Brines. Corrosion, 71 (12). pp. 1452-1466. ISSN 0010-9312

https://doi.org/10.5006/1770

The influence of pH on localized corrosion behaviour of X65 (UNS K03014) carbon steel in CO_2-saturated brines

Frederick Pessu, Richard Barker and Anne Neville
Institute of Functional Surfaces (iFS)
School of Mechanical Engineering,
University of Leeds, Leeds, LS2 9JT, UK

ABSTRACT

Pitting and localized corrosion of carbon steel is considered to be a complex process influenced by a wide range of parameters such as temperature, bulk solution pH and chloride ion concentration. Solution pH is known to influence corrosion product characteristics and morphology in CO_2 and H_2S-containing corrosion systems. However, from the perspective of pitting corrosion in CO_2-saturated environments, the extent to which bulk pH of solutions and the presence of corrosion products influence localized attack is still not clearly understood. This paper presents an investigation into the role of pH on the characteristics of corrosion product and pitting corrosion behavior of X65 carbon steel in CO_2-saturated brine. Pitting corrosion studies were conducted over 168 hours at 50°C in 3.5 wt.% NaCl solutions at different bulk pH (buffered to pH values of 6.6 and 7.5 in some cases) in order to understand and correlate the role of pH on corrosion product morphology, chemistry, initiation and propagation of pits within each distinct environment. Corrosion product composition and morphology are identified through a combination of electrochemical and surface analysis techniques, which include Scanning Electron Microscopy (SEM) and X-Ray Diffraction (XRD). The extent of corrosion damage of the carbon steel is evaluated through the implementation of surface interferometry to study discrete pit geometry; namely, the size, depth and aspect ratio. Results indicate that the process of pit initiation and propagation of carbon steel in CO_2 corrosion environment is different depending upon bulk solution pH. At low pH (pH values starting at 3.8), pitting initiates faster and propagates steadily along with significant uniform corrosion due to the formation of 'amorphous' form of $FeCO_3$. At higher pH, uniform corrosion is significant, while pitting initiates with increasing protection from crystalline $FeCO_3$. At a pH value of 7.5, pitting corrosion initiation occurs after and/or during pseudo-passivation is achieved due to the formation of a 'protective and pseudo-passivating' $FeCO_3$ film.

KEY WORDS: CO_2 corrosion, corrosion products, uniform corrosion, pitting, pseudo-passivation, iron carbonate, iron carbide

INTRODUCTION

The mechanisms associated with the dissolution of carbon steel in CO_2-containing environments have been debated for decades. Various models have been developed and published in the literature that attempt to take into account the number of parameters which influence corrosion rate [1, 2]. Regrettably, these models often appear contradictory to one another and can span over two orders of magnitude in the predicted corrosion rate for the same input parameters [2, 3]. This disparity lies in how the various parameters are treated and how much conservatism and sensitity to environmental parameters is integrated into each model. For example, the NORSOK standard M-506 model is one of the open source models for corrosion rate prediction with a greater sensitivity to solution pH than the de Waard models [1].

Dugstad [2] stated that it is important to understand that the term "CO_2 corrosion" and the effect of CO_2 is not related to solely one mechanism. A wide range of electrochemical, chemical and mass transport processes; such as H_2CO_3 reduction reaction, H_2O reduction and hydrogen-evolution etc [4, 5], are occurring simultaneously at the interface of the corroding steel and the electrolyte. The majority of these reactions are sensitive to changes in the fluid properties (temperature, pressure, brine chemistry) and the flow conditions (velocity, flow regime), making the process incredibly complex in some instances, especially when localized attack occurs.

One of the key factors influencing both general and localized corrosion rates of carbon steel in CO_2-containing brines is the nature and morphology of surface corrosion products. These corrosion products can consist of undissolved portions of the steel surface (such as Fe_3C), or they can form on the steel surface via precipitation reactions (such as $FeCO_3$). In some instances, carbon steel has also been shown to enter a pseudo-passive regime at higher pH [6, 7].

Considering the fact that pH plays a critical role in influencing both the kinetics of corrosion reactions [4, 8] as well as the morphology and composition of corrosion products [8, 9], it is expected that the initiation and propagation of pitting corrosion is affected by bulk pH of corrosion environments. The present paper focuses on the effect of three different corrosion environments buffered using sodium bicarbonate ($NaHCO_3$) to different levels of bulk pH but in the same 3.5 wt. % NaCl brine solution. Temperature and partial pressure of CO_2 are kept constant at all times.

Film morphologies on carbon steel observed in CO_2 corrosion

The rationale behind the selection of the three pH values (pH = 3.8 (unbuffered), 6.6 and 7.5) was to promote the evolution of three distinctly different corrosion environments, corrosion products and evaluate the role of these corrosion products and the respective environments on the localized and general corrosion behavior of carbon steel. The following literature review therefore highlights the various corrosion product morphologies that can exist on carbon steels in CO_2-containing environments in order to justify the selection of pH values considered in this work. The three types of corrosion products sought were:

(i) Non-protective iron carbide (Fe_3C) corrosion product layer composed of little or no trace of crystalline $FeCO_3$ corrosion products.

(ii) A protective and crystalline form of $FeCO_3$ film capable of reducing the uniform corrosion rate to 0.1 mm/yr.

(iii) A highly protective $FeCO_3$ film with pseudo-passive characteristics believed to be attributed to magnetite (Fe_3O_4) [6].

In the experiments performed within this work, the goal was to maintain the partial pressure, temperature and chloride ion concentration in the bulk solution, varying only the bulk pH. This would enable identification of the role pH plays on surface corrosion product formation and the resulting effect this has on the general and localized corrosion behavior of the underlying substrate. The following review considers literature on the formation of Fe_3C, $FeCO_3$ and Fe_3O_4 corrosion products.

<u>Iron carbide (Fe_3C) films</u>

Fe_3C is commonly observed on the surfaces of carbon steel subjected to CO_2 corrosion and the development of a porous network has been typically observed on steels with a carbon content in excess of 0.15% [10, 11]. An Fe_3C network is revealed on steel surfaces as a result of the preferential dissolution of the α-ferrite phase within the steel microstructure. Fe_3C is also believed to be able to

act as an electronic conductor which is capable of accelerating the corrosion rate of carbon steel by inducing a galvanic effect on the steel surface and acting as a favorable cathodic site for hydrogen evolution [12, 13]. Dugstad [14] identified that ferritic-pearlitic microstructures can result in the evolution of a porous carbide layer, which remains uncorroded when exposed to CO_2 environments. Farelas et al [10] attributed the significant increase in corrosion rate to the presence of Fe_3C which generates cathodic sites with a lower overpotential for hydrogen evolution [12].

For the experiments conducted in this work, to obtain a non-protective corrosion product layer consisting of mainly Fe_3C on the carbon steel surface, whilst also ensuring minimal precipitation of $FeCO_3$, a pH value of 3.8 (unbuffered) was chosen along with a temperature of 50°C. Such conditions would ensure that if supersaturation was indeed reached, the precipitation rate would be slow and theoretically not influence the corrosion rate of the underlying substrate significantly.

Iron carbonate ($FeCO_3$) corrosion products

$FeCO_3$ is capable of dramatically influencing the corrosion kinetics of the underlying steel via the precipitation of a crystalline layer on the steel surface and acting as a diffusion barrier to electrochemically active species involved in the charge-transfer process. The protectiveness of the film is influenced by several environmental factors such as temperature, pH, partial pressure and ferrous ion concentration. $FeCO_3$ is able to precipitate via a one-stage reaction with carbonates, or via a two-stage reaction with bicarbonates:

$$Fe^{2+} + CO_3^{2-} \rightarrow FeCO_3 \quad (1)$$

$$Fe^{2} + 2HCO_3^{-} \rightarrow Fe(HCO_3)_2 \quad (2a)$$

$$Fe(HCO_3)_2 \rightarrow FeCO_3 + CO_2 + H_2O \quad (2b)$$

It is well known that pH has a strong influence on the solubility of $FeCO_3$. Saturation of a saline solution with ferrous ions is achieved with 100 times less ferrous ions per unit increase in the bulk pH of the corrosion environment [2]. Therefore, based on these premise a pH of 6.6 was chosen at 50°C in this study in order to form protective and crystalline $FeCO_3$.

Pseudo-passive film (iron carbonate ($FeCO_3$) and magnetite (Fe_3O_4))

It has been demonstrated that in addition to the generation of $FeCO_3$ corrosion product, the steel surface can enter into a pseudo-passive state, facilitating significant corrosion protection. The pseudo-passivation process results in a significant ennoblement of the carbon steel open circuit potential (by a magnitude ranging between 400 and 800 mV in some instances [7]). It was postulated by Han et al [7] that the formation of the pseudo-passive corrosion products, could establish a galvanic cell on the carbon steel between the corrosion product covered pseudo-passive area and the actively corroding bare steel.

In terms of selection of pH to achieve pseudo-passivation in this study, Han et al [7] reviewed the passivation of X65 steel in 1 wt.% NaCl brine at 50°C and a pH of 7.5 in a static solution and observed that the steel entered a pseudo-passive state after 1 to 2 days of exposure. Consequently, the aforementioned conditions were chosen in the hope that passivation would occur early in the stages of the 7 day test to determine the influence of passivation on general and localized corrosion.

EXPERIMENTAL PROCEDURE

Experimental setup: Figure 1 shows a schematic of the bubble cell apparatus used for the CO_2 corrosion experiments. Experiments were conducted in two vessels which were each filled with 2 litres of 3.5 % NaCl brine.

Materials and preparation: The steels specimens placed in the vessels consisted of 10 mm x 10 mm x 5 mm X65 (UNS K03014) carbon steel samples. The steel was in a normalized form and consequently possessed a ferritic/pearlitic microstructure. The composition of X-65 steel is provided in Table 1.

Table 1: X65 Carbon steel composition (wt. %)

C	Si	P	S	Mo	Mn	Ni	Nb	V	Fe
0.15	0.22	0.025	0.002	0.17	1.422	0.09	0.054	0.057	97.81

Wires were soldered to the back of all the test specimens before embedding them in a non-conducting resin. Prior to the start of each experiment, all test samples were wet ground with 1200 silicon carbide grit paper, degreased with acetone, rinsed with distilled water and dried with compressed air before immersion into the test solution. A sample surface area of 1 cm^2 was exposed to the electrolyte per sample and 10 samples were immersed in each 2 litre vessel. Each experiment was conducted for 168 hours and two samples were removed from each solution after 7, 36, 72, 120 and 168 hours for scanning electron microscopy (SEM)/X-ray diffraction (XRD) analysis to assist in observing the evolution of the surface corrosion products and pitting corrosion characterization.

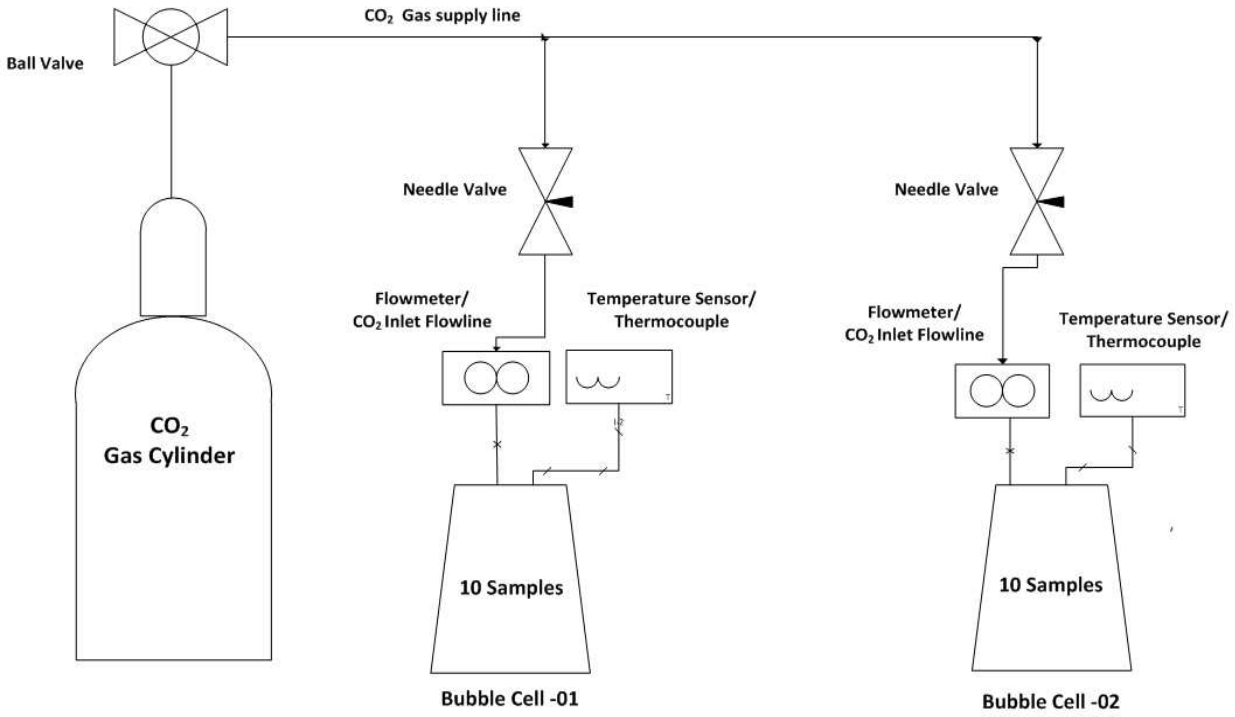

Figure 1: Schematic of the test cells for CO_2 corrosion testing

Brine preparation and test conditions: The test solution (3.5 wt. % NaCl solution) was completely saturated with CO_2 for a minimum of 12 hours prior to starting each experiment to reduce oxygen concentration down to 20 ppb, simulating oilfield environments. CO_2 was also bubbled into the system throughout the duration of every experiment and all tests were conducted at atmospheric pressure. The temperature in all experiments was kept constant at 50 ± 1°C whilst solution pH was

varied for each experiment and controlled through the addition of sodium bicarbonate (see Table 2 for approximate quantities of Sodium bicarbonate used to achieve each pH levels).

Based on the literature review performed, three pH values; unbuffered test environment with pH starting at 3.8, pH of 6.6 and pH of 7.5 were evaluated in an effort to create three distinctly different corrosion films; an Fe_3C network with non-crystalline form of $FeCO_3$, crystalline and protective form of $FeCO_3$ and protective form of $FeCO_3$ with pseudo-passivating properties respectively and which would all theoretically offer varying levels of general corrosion protection to the substrate.

Table 2: $NaHCO_3$ required for different levels of pH for in a 3.5 wt. % solution at 50°C

pH	Amount of $NaHCO_3$ used as buffer (g) per 2L solution
3.8	Nil
6.6	≈10
7.5	≈250

In-situ electrochemical measurements: All experiments were conducted in a twin vessel as shown in Figure 1 to ensure repeatability of electrochemical and pitting corrosion data. Electrochemical measurements were conducted on two samples out of the 10 samples per test cell and these samples remained within the vessels until the end of the experiment to allow full collection of electrochemical data over the entire 168 hours. The average of four in-situ linear polarization measurements from a minimum of three repeatable experiments is presented in the discussion section. It is important to note that experiments were also repeated up to four times in some instances in order to obtain four repeatable LPR measurements. Each sample formed the working electrodes in a three-electrode cell which also comprised of an Ag/AgCl reference electrode and a platinum auxiliary electrode. Corrosion rate measurements were conducted using both DC and AC measurements with a potentiostat. For each long term experiment, two samples were subsequently removed from each test cell at sampling times of 7, 36, 72, 120 and 168 hours to enable the evolution of corrosion products and the growth of surface pits to be examined.

In terms of DC techniques, linear polarization resistance (LPR) measurements were performed by polarizing the working electrode from 15 mV below the open circuit potential (OCP) to 15 mV more positive than the open circuit potential (OCP) at a scan rate of 0.25 mV/s to obtain a polarization resistance (R_p). Tafel polarization curves were generated based on poteniodynamic measurements performed on freshly polished samples in separate tests at each solution pH to determine anodic and cathodic Tafel constants and ultimately the Stern-Geary coefficient, which was subsequently used in conjunction with Faraday's Law and the measured values of R_p to estimate general corrosion rates. Tafel plots were obtained by performing anodic and cathodic polarization sweeps on two different samples in the same test cell. Scans always started at the OCP and extended ±250 mV at a scan rate of 0.25 mV/s. Both anodic and cathodic sweeps were performed on separate samples to ensure reliable measurements. Tafel polarization measurements were performed at varying times prior to film formation at stable corrosion potentials; usually after LPR measurements up to 7 hours.

Characterization of pitting corrosion damage: Corrosion tests were conducted for 168 hours with the aim of monitoring the growth of different morphologies of corrosion products and assessing the impact these had on the initiation and propagation of surface pitting. Pit depth measurements were conducted in alignment with ASTM G46-94 [15]. A 3D interferometer was used in this study for defining the discrete geometry of pits on almost the entire steel sample surface area (≈ 81% of $1cm^2$ sample). Pits were identified based on carefully chosen thresholds with distinct pit depths, diameters, and areas being quantified. ASTM G46-94 stipulates that an average of the 10 deepest pits and the maximum pit depth (based on relative pit depth measurement after removal of corrosion products) should be used for the characterization of pitting corrosion damage. A sample surface area of 9 x 9 mm^2 was analyzed for pits from the 10 x 10 mm^2 sample and a systematic

stitching approach was adopted whereby 9 different 3 x 3 mm^2 areas were stitched together. Consequently, 3D images of regions where the deepest pits exist are identified on the sample surface with a high degree of accuracy and resolution.

It is very important to note here that there is no generally accepted consensus on the minimum dimensions a pit can take in terms of depth and diameter, especially in non-passivating alloys like carbon steels. However, there are various suggestions of the different possible shapes, orientations and sizes of pits in ASTM G46-94 [15]. Nonetheless, attempts have been made in this work to provide visual evidence of pits/cavities in terms of the maximum pits identified by the techniques implemented in this work. Such examples are provided later in this paper.

RESULTS

Tafel plot, corrosion rate and open circuit potential observations: Figure 2 shows the Tafel plots obtained by performing separate anodic and cathodic polarization sweeps about the OCP of X65 steel after 7 hours of immersion in the test solution. The graphs correspond to solutions of pH starting at 3.8 (unbuffered), 6.6 and 7.5. Table 3 indicates the measured Tafel constants and the resulting Stern-Geary coefficient which was used with the polarization resistance (R_p) and Faraday's Law to determine corrosion rate as a function of time, after taking into account solution resistance (which ranged between 4-7 Ohm.cm^2). Figure 2 indicates signs of pseudo-passivation occurring on the steel surface exposed to the solution at pH 7.5 at higher anodic potentials; the current reaches a maximum at ≈ -540 mV and is shown to decrease as the potential is further increased. The cathodic reaction lines shows a diffusion limiting cathodic current contributed to by the reduction of H^+ and potentially H_2CO_3 as expected at lower pH, while at higher pH values the cathodic reaction is influenced more by water reduction with less H^+ in the corrosive media. These results show good consistency with results by several authors [4, 16].

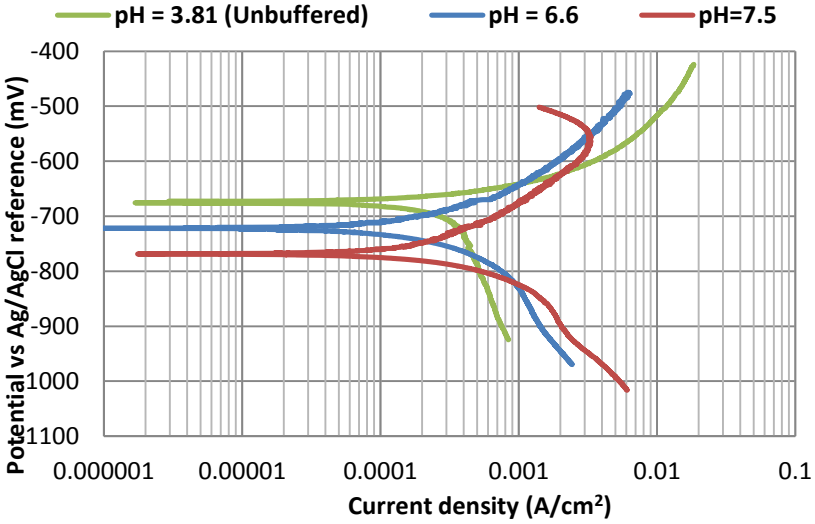

Figure 2: Tafel plots for X65 carbon steel in 3.5 wt.% NaCl solutions at 50°C and pH values of 3.8, 6.6 and 7.5

Table 3: Tafel constants at different levels of pH for X65 in a 3.5 wt.% solution at 50°C

pH	β_a (mV/decade)	β_c (mV/decade)	B (Stern-Geary Coefficient) (mV/decade)
3.8 (unbuffered)	40	168	14
6.6	80	95	19
7.5	95	100	21

Referring to Figure 3(a), at a starting pH of 3.8 the corrosion rate increases with time, before reducing slowly and stabilizing at 2.8 mm/year between 72 and 168 hours. At pH 6.6, the corrosion rate reduces continuously over the test duration, reaching a final corrosion rate of 0.09 mm/year after 168 hours. At pH 7.5, the initial corrosion rate is in excess of 3.5 mm/year but reduces rapidly to values of approximately 0.02 mm/year after 20 hours. Referring to Figure 3(b), the point where the lowest corrosion rate is reached coincides with the passivation of the steel surface at pH 7.5, which is indicated by the increase in potential of the steel surface from -770 to in excess of ≈ -250 mV. The corrosion environment at pH of 7.5 at the start of experiment was initially higher than at lower pH. The reason for the higher initial corrosion rate at this pH value is still not clear, but there is evidence in the literature [7] that suggests the idea of a certain pH threshold above which the corrosion rate of carbon steel may become high again potentially due to the direct reduction of carbonate and bicarbonate ions. As stated previously, the passivation after 1-2 days was expected given the similarity between these conditions and those investigated by Han et al [7].

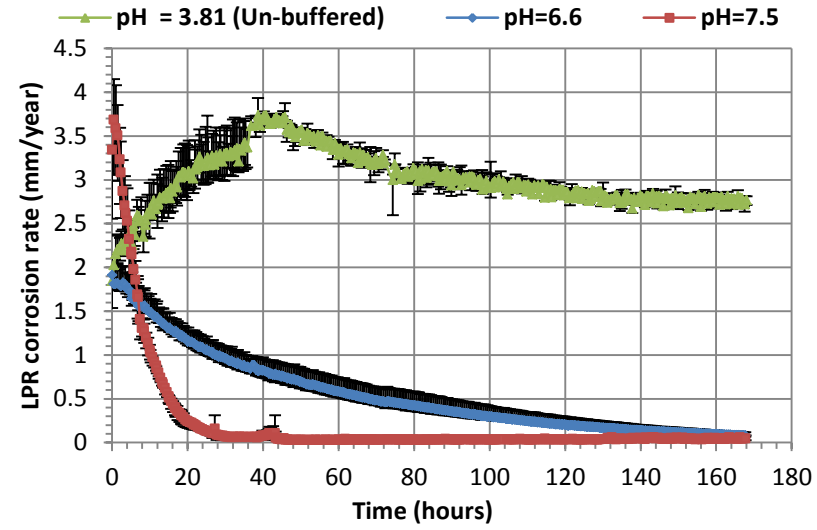

(a)

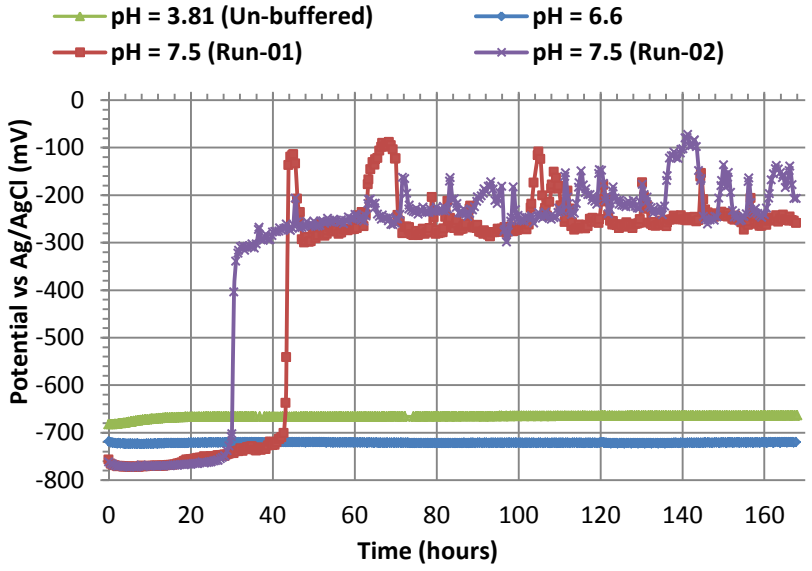

(b)

Figure 3: (a) LPR corrosion rate and (b) OCP over 168 hours for X65 carbon steel in a 3.5 wt.% NaCl solution at 50°C and solution pH values of 3.8 (unbuffered), 6.6 and 7.5. All graphs represent averages of four data points from repeatable experiments except the OCP reading for pH 7.5, where repeats are shown individually for clarity due to the passivation process.

Linking corrosion behavior to corrosion product surface morphology: For each experiment conducted at a starting pH of 3.8 (unbuffered), 6.6 and 7.5, the samples were removed from the brine after 7, 36, 72, 120 and 168 hours. Each sample was analyzed using the SEM to track the growth of surface corrosion products and correlate such to the electrochemical response.

Starting pH of 3.8 (unbuffered)

SEM images of the X65 surface when exposed to the solution at a starting pH 3.8 are provided in Figure 4. From Figure 3, over the first 7 hours the corrosion rate rises in conjunction with a slight initial increase in OCP. Figure 4(a) indicates the presence of Fe_3C on the entire steel surface after 7 hours which is believed to be predominantly responsible for the change in corrosion rate and corrosion potential by promoting the cathodic reaction on the steel surface [11, 12, 17]. After 36 hours, corrosion rates reach a maximum and begin to reduce in conjunction with the evidence of the formation of a 'smudge-like textured' corrosion product on the steel surface (shown in Figures 4(b) to (d)). The development of this surface film has been identified in a previous publication [18] and was found to consist of nano-crystalline or an amorphous like form of $FeCO_3$ through the implementation of selected area electron diffraction and energy dispersive X-ray analysis using a transmission electron microscope. The evidence of the presence of an amorphous form of $FeCO_3$ during this period also coincided with an increase in bulk pH from 3.8 at the start of experiment to 4.6 after 36 hours. According to Guo et al [19], the increase in bulk pH is due to the buffering effect from the ferrite dissolution process, which is expected to exceed the rate of $FeCO_3$ formation in the initial stages of the corrosion process. The buffering effect continued until after 72 hours after which the pH stabilizes at ≈ 5.0 up to the end of the test. The amorphous layer is shown to build up over time along with some localized crystals of $FeCO_3$ up to 168 hours, after which the corrosion rate stabilizes at approximately 2.8 mm/year. It appears that the amorphous film is capable of offering slight protection to the steel surface.

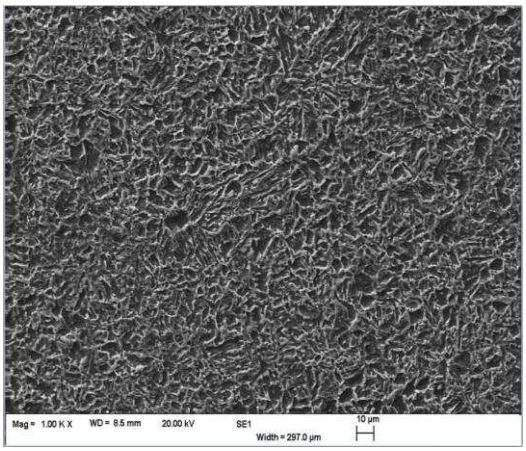

(a) After 7 hours exposure

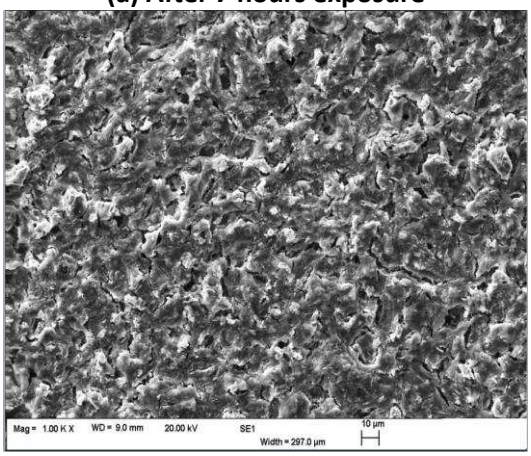

(b) After 36 hours exposure

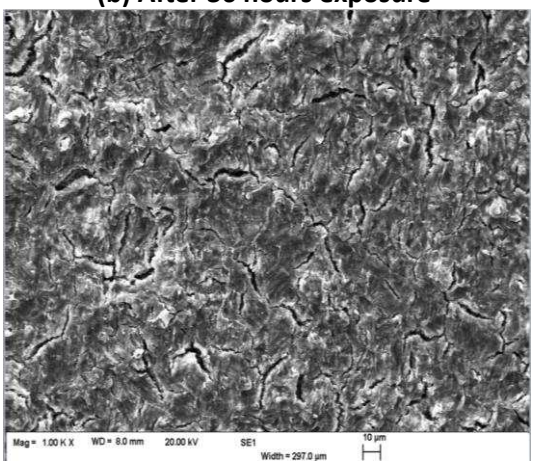

(c) After 72 hours exposure

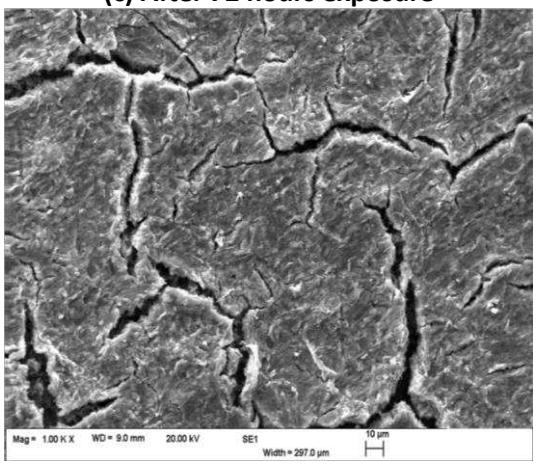

(d) After 168 hours exposure

Figure 4: SEM images of surface films present on X65 carbon steel after exposure to 3.5 wt.% NaCl solution at 50°C and pH of 3.8 for a period of (a) 7 hours, (b) 36 hours, (c) 72 hours and (d) 168 hours

pH 6.6

SEM images of the X65 steel surface after exposure to the solution at pH 6.6 for 7, 36, 72 and 168 hours are provided in Figure 5. Increased bulk solution pH has resulted in the formation of $FeCO_3$ crystals which have already nucleated on the steel surface after 7 hours (Figure 5(a)). The increase in bulk pH significantly decreases the solubility of $FeCO_3$, resulting in its precipitation. In these particular conditions, Dugstad [2] determined that the solubility of ferrous ions required is only a fraction of a ppm, as opposed to over 100 ppm in the bulk solution at pH 3.8. Consequently, $FeCO_3$ precipitation is far more favorable at the higher pH and has resulted in the formation of a crystalline corrosion product layer.

After 36 hours of exposure, discrete crystals of $FeCO_3$ are evident on the steel surface from 1-2 µm to over 10 µm in width (Figure 5(b)). In conjunction with this behavior, the corrosion rate is also declining over this period as a result of the $FeCO_3$ crystals blocking some active sites on the steel surface. From 36 hours onwards, there is continued nucleation and growth of the $FeCO_3$ crystals which resulted in a substantial corrosion product layer being formed. From this point onwards, the $FeCO_3$ film has the ability to also act as a diffusion barrier to electrochemically-active species involved in the charge-transfer reaction through the generation of a protective corrosion product on the steel surface. By considering Figures 5(c) and (d), it is evident that areas still exist on the steel surface through which the electrolyte could have a direct pathway to the steel surface (see Figure

5(d) in particular). However, extensive SEM analysis indicated that the number and size of these localized regions did reduce significantly from 72 to 168 hours as crystals continued to grow.

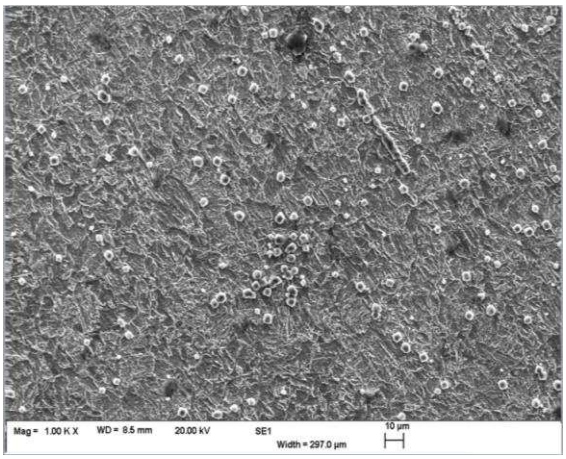

(a) After 7 hours exposure

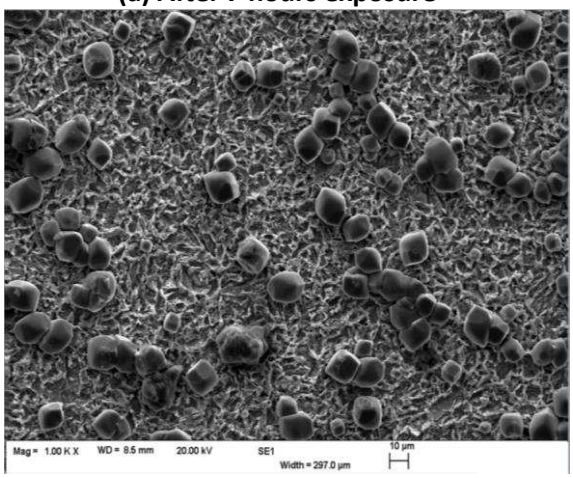

(b) After 36 hours exposure

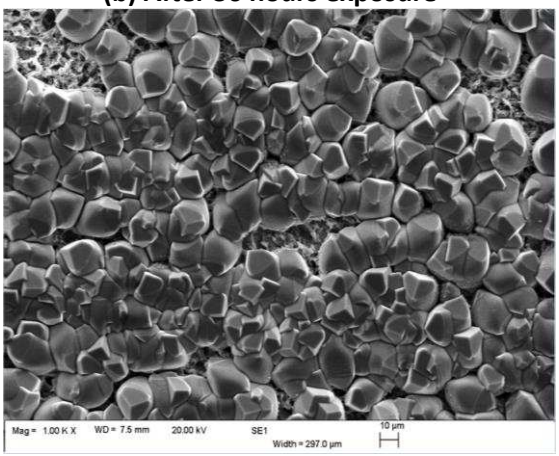

(c) After 72 hours exposure

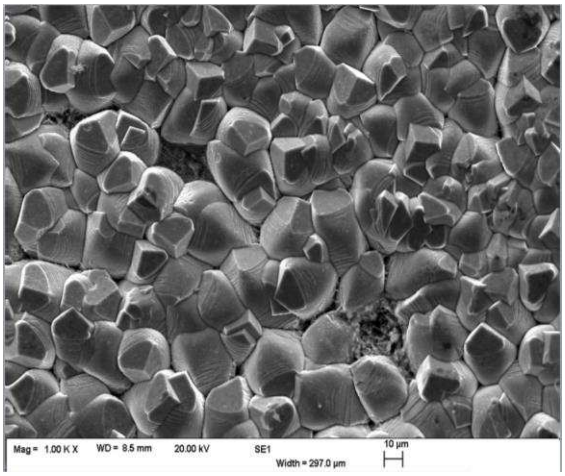

(d) After 168 hours exposure

Figure 5: SEM images of surface films present on X65 carbon steel after exposure to 3.5 wt.% NaCl solution at 50°C and pH of 6.6 for a period of (a) 7 hours, (b) 36 hours, (c) 72 hours (d) 168 hours

pH 7.5

SEM images of the X65 steel surface exposed to the solution at a pH of 7.5 after 7, 36, 72 and 168 hours are provided in Figure 6. A further increase in system pH resulted in even more substantial levels of $FeCO_3$ precipitation occurring earlier in the experiment. This was attributed to a further reduction in the solubility of $FeCO_3$ in the bulk solution as a result of the increase in pH.

Pseudo-passivation is observed to have occurred between 20 and 40 hours as shown by a shift in the corrosion potential from ≈ -770 mV to ≈ -250 mV in Figure 3(b). No significant change in the top view morphology of the film was observed between 36 and 72 hours, other than the size of $FeCO_3$ crystals becoming larger. It has been suggested that the pseudo-passivation effect occurs underneath the corrosion product [20]. Regrettably, the nature of this layer responsible for the pseudo–passivation effect according to Han et al [20] could not be identified using XRD in this study and is the subject of continuing research. However, it is clear that 'pseudo-passivation' had occurred based on the significant change in corrosion potential. As mentioned previously, it has been suggested by Han et al [20] that the pseudo-passive layer could comprise of magnetite (Fe_3O_4). According to Han et al [20], The formation of Fe_3O_4 in CO_2 corrosion environment was thought to be favored by the reactions;

$$3Fe + 4H_2O \rightarrow Fe_3O_4 + 8H^+ + 8e^- \qquad 3(a)$$

$$3FeCO_3 + 4H_2O \rightarrow Fe_3O_4 + 3HCO_3^- + 5H^+ + 2e^- \qquad 3(b)$$

According to Han et al [20], the tendency for formation of magnetite via Eq.3(a) is influenced by a critical pH. Han et al [7] also demonstrated that the pH value at the surface of the steel can be significantly higher than that in the bulk solution, making pseudo-passivation (potentially by the presence of Fe_3O_4) more favorable.

After 7 hours of exposure (Figure 6(a)), a significant proportion of the surface was covered in $FeCO_3$ crystals which possessed a very different structure to those observed at pH 6.6. The crystals formed at pH 7.5 consist of a platelet structure with sharper, more defined edges and corners as opposed to the rounded crystals observed in at pH 6.6.

After 36 hours of exposure, the entire surface was almost entirely covered by $FeCO_3$ crystals. Very little changes were observed from the top view SEM images from 36 hours onwards. The only noticeable change was an increase in crystal size.

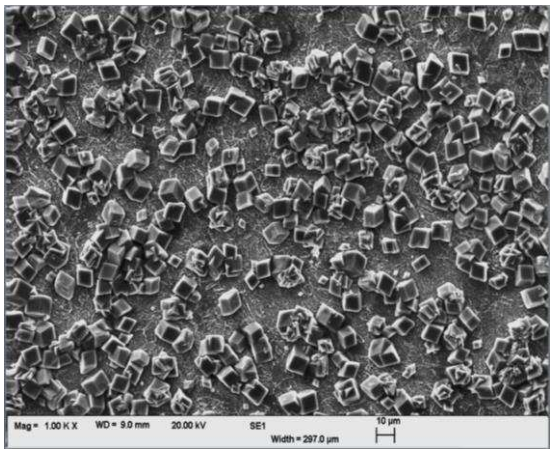

(a) After 7 hours exposure

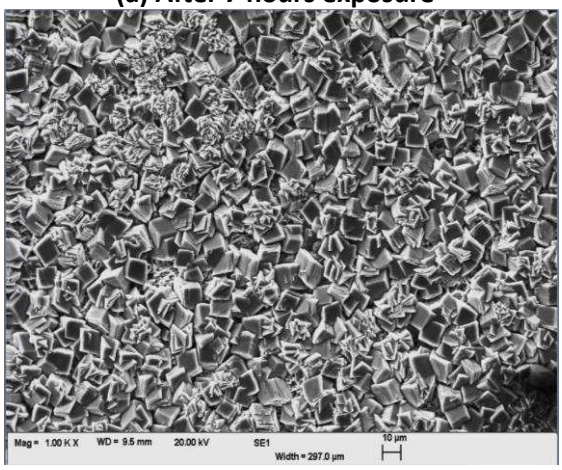

(b) After 36 hours exposure

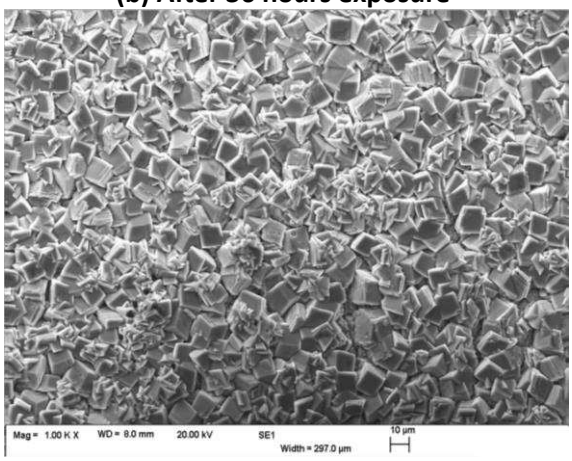

(c) After 72 hours exposure

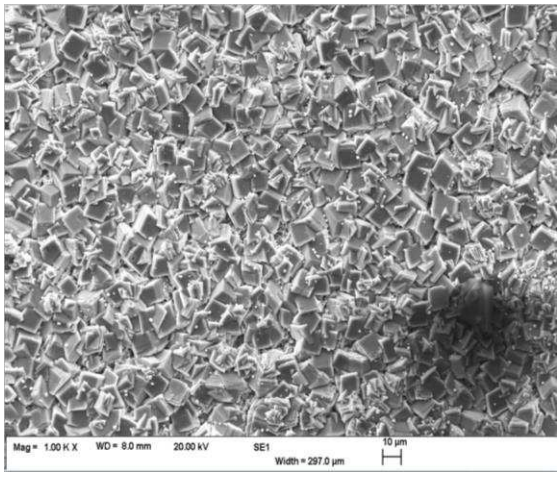

(d) After 168 hours exposure

Figure 6: SEM images of surface films present on X65 carbon steel after exposure to 3.5 wt.% NaCl solution at 50°C and pH of 7.5 for a period of (a) 7 hours, (b) 36 hours,(c) 72 hours and (d) 168 hours

Figure 7 shows the reference XRD patterns for Fe, Fe_3C and $FeCO_3$, while Figure 8 shows the XRD pattern [21-23] for the corrosion product layer for carbon steel in 3.5 wt. % NaCl solutions at 50˚C after 168 hours at pH 3.8 (unbuffered), 6.6 and 7.5. The XRD patterns in Figure 8 confirm the formation of an extensive layer of crystalline $FeCO_3$ at pH 6.6 and 7.5, while at pH of 3.8; the corrosion product layer is dominated by a non-crystalline form of $FeCO_3$.

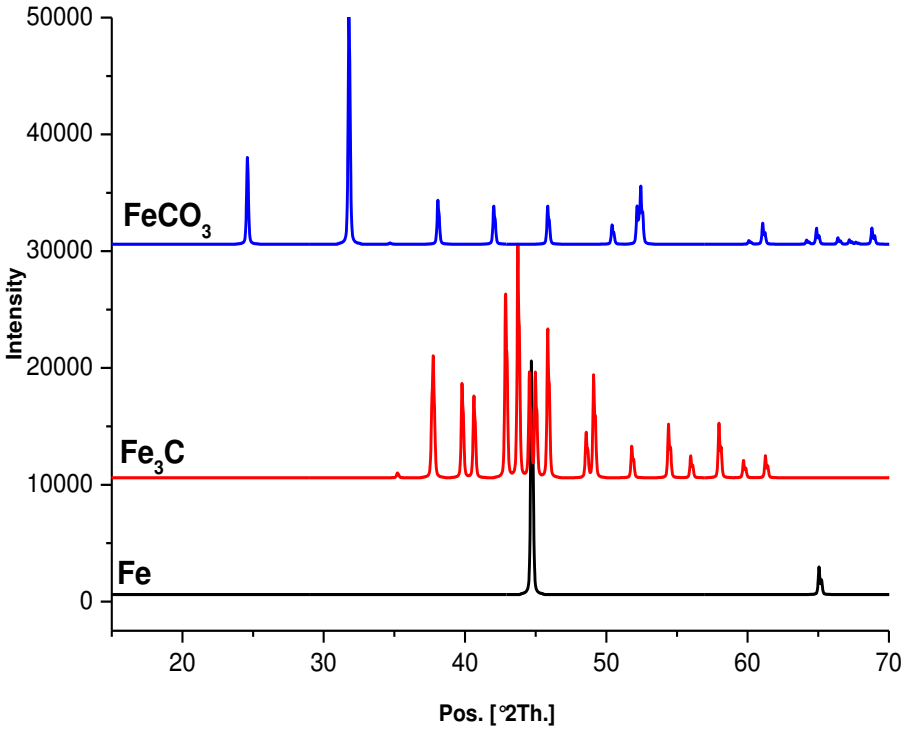

Figure 7: Reference XRD patterns for Fe, Fe_3C and $FeCO_3$ [21-23]

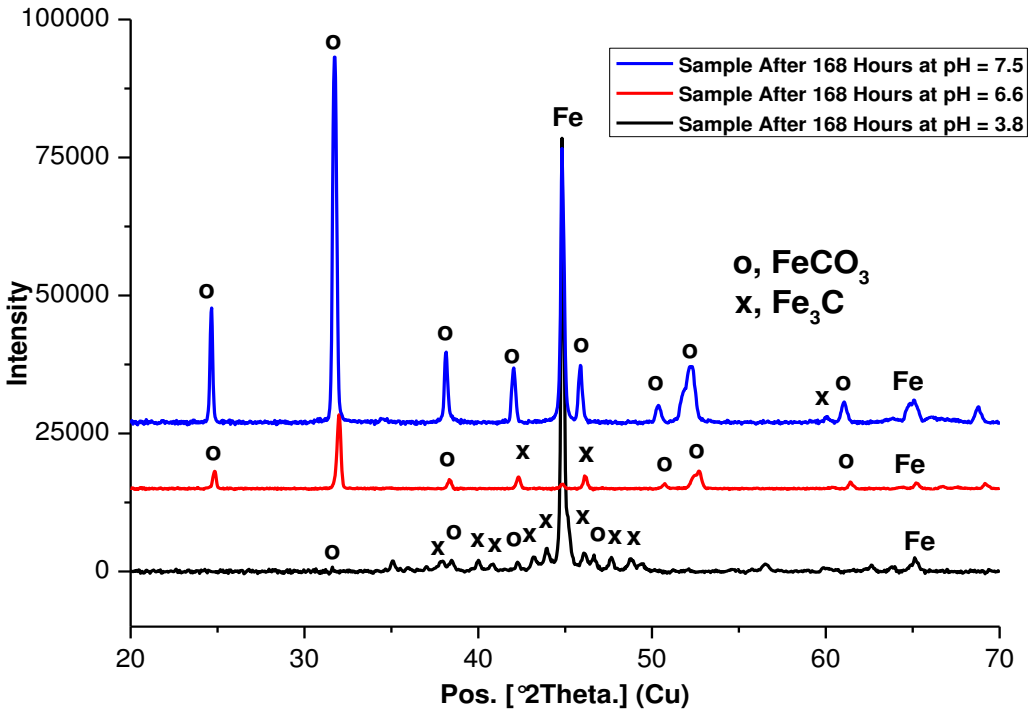

Figure 8: XRD pattern of corrosion product film on carbon steel samples in a 3.5 wt.% NaCl brine after 168 hours at different pH.

Linking pitting behavior to surface morphology, corrosion rate and corrosion potential: The main focus of this research is to understand and establish the correlation between the pitting corrosion behavior of carbon steel pipeline material with the corrosion product morphology and electrochemical responses as influenced by the bulk pH of the solution. Figure 9 shows the maximum and average pit depths measured on the sample surface in relation to the LPR corrosion rate and OCP measurements for each test performed at pH values of 3.8 (unbuffered), 6.6 and 7.5.

Referring to the tests at pH 3.8 (Figures 9(a) and (b)); pit growth is continuous and relatively linear throughout the entire experiment. The formation of the non-protective and amorphous-like $FeCO_3$ appears to have little or no influence on reducing pit growth. Similar trends has been observed in a previous publication [18]. This behavior is logical given that the film has had little impact on reducing the general corrosion rate on the steel surface. A maximum pit depth of 50 µm was recorded by the end of the experiment.

Experiments performed at pH 6.6 (Figures 9(c) and (d)) show a marked difference in comparison to those at pH 3.8. Pit growth over the first 72 hours is very slow, where only a depth of 13 µm is reached (half that at pH 3.8 after the same exposure time). Interestingly, between 72 and 120 hours, there is a significant increase in pit depth. The observed pit growth occurs in conjunction with the high degree of surface coverage of the $FeCO_3$ corrosion products, as shown in the SEM images in Figure 5. It is suggested that the small cavities in the $FeCO_3$ corrosion products have resulted in the increase in regions of localized attack and the accelerated growth in pit depth. Once these voids become filled through further precipitation, the pit growth is likely to be retarded as shown in the pit depth values at 168 hours. The formation of the extensive $FeCO_3$ corrosion product layer appears to be reducing the pit propagation.

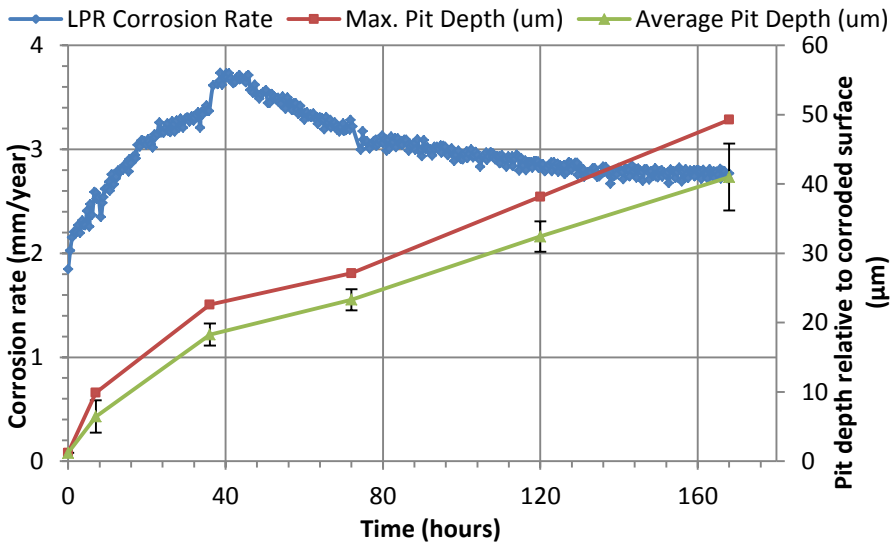

(a) At a starting pH of 3.8 (unbuffered)

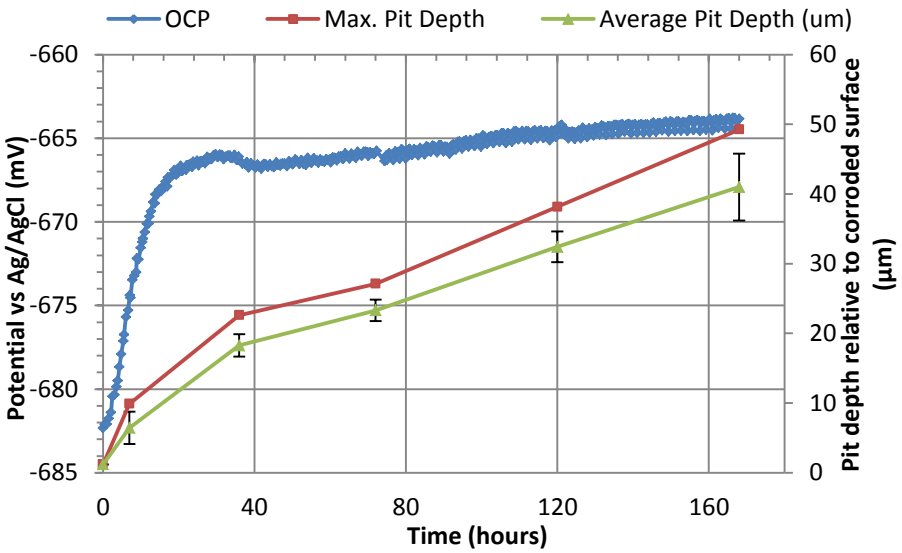

(b) At a starting pH of 3.8 (unbuffered)

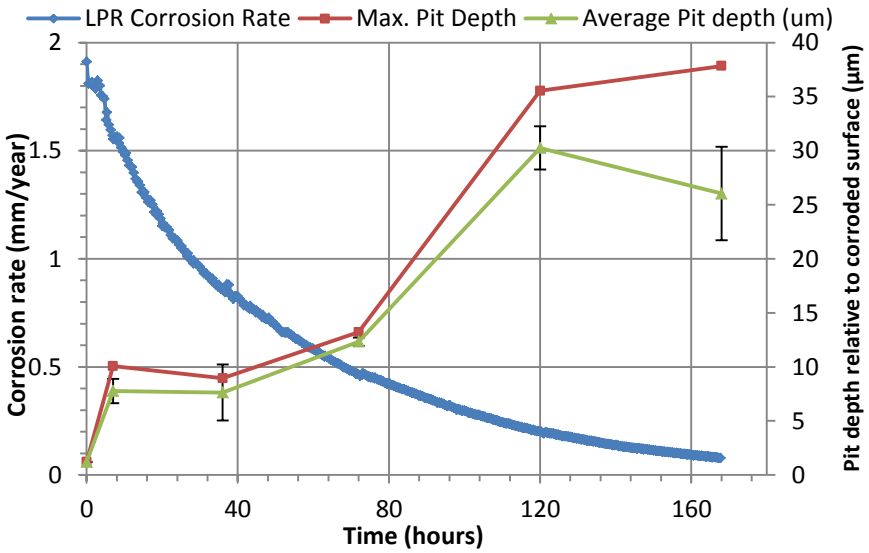

(c) At pH of 6.6 (buffered)

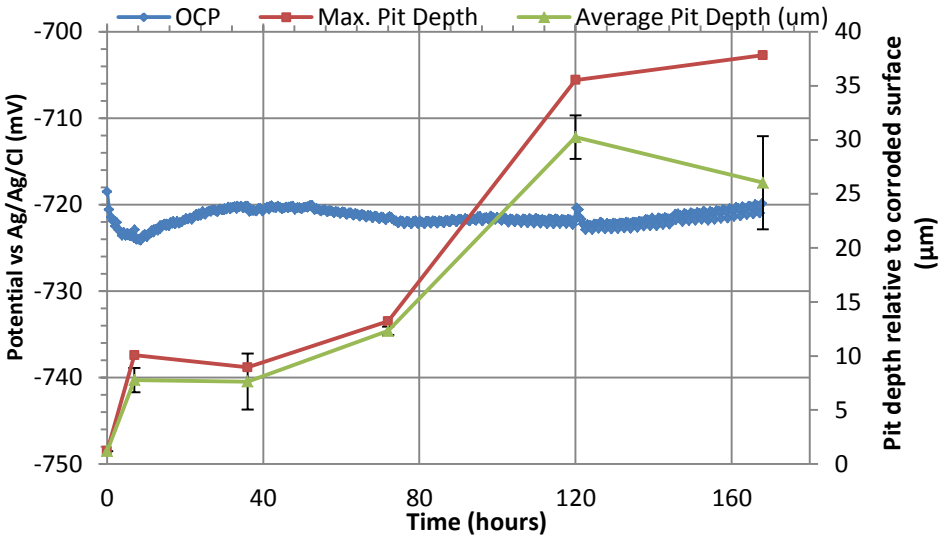

(d) At pH of 6.6 (buffered)

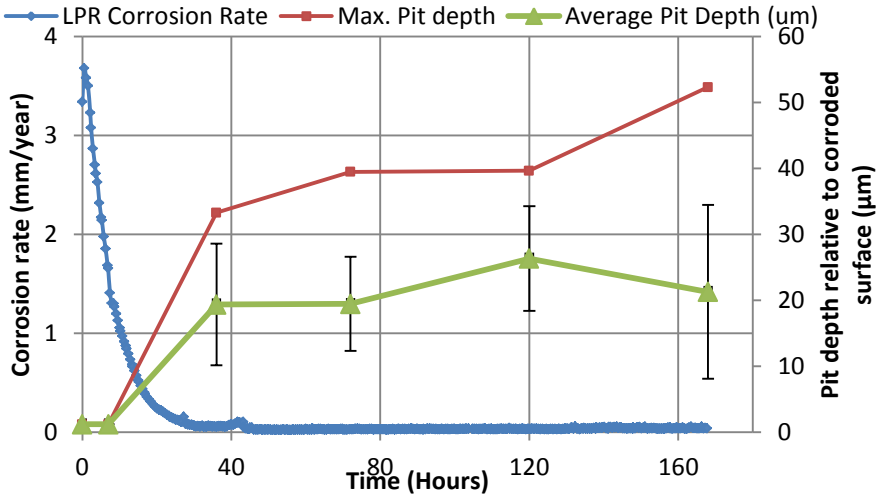

(e) At pH of 7.5 (buffered)

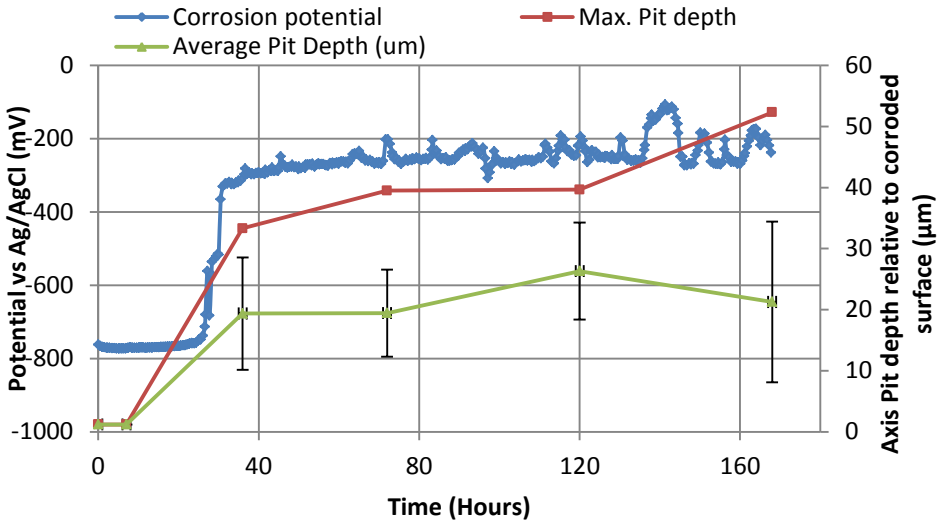

(f) At pH of 7.5 (buffered)

Figure 9: Pit growth in conjunction with LPR corrosion rate and OCP measurements for (a) and (b) pH 3.8; (c) and (d) pH 6.6; (e) and (f) pH 7.5.

At pH 7.5, the average of the 10 deepest pits presented in Figures 9(e) and (f) is significantly lower than the maximum pits due to the limited number of pits identified on the steel surface above 10µm. The results also indicate that the size distribution of pits varies with changing pH. This is evident from the standard deviation plotted as error bars. After 7 hours, no pits were identified on the entire steel surface. However, after the pseudo-passivation process, pits in excess of 30 µm deep were clearly recorded. By considering the maximum pit depths, it appears that pit growth continues under the pseudo-passive regime, but at a much slower rate than that recorded at pH 3.8, although this requires further research to come to a firm conclusion. The results suggest in this instance, that the pseudo-passivation process results in the initiation and propagation of pits on the steel surface, but once OCP stabilizes, the rate of pit growth is not as fast as the test at pH 3.8. Further research is required to explore the relationship between OCP and pit growth when pseudo-passivation of steel occurs.

Concept of total pit penetration rate and pitting factor: When considering the threat posed to carbon steel pipework subject to pitting corrosion, the potential failure mechanism of a pipeline that is suceptible to pitting will not only depend upon the rate at which pits propagate *relative* to the corroding surface, but also on the uniform corrosion rate of the surrounding area. Total metal penetration (P_d), also refereed to as 'absolute' pit depth is defined as the sum of the pit depth relative to the corroded surface (d_{max}), plus the average metal loss from general corrosion rate measurements (termed P_u), i.e. $P_d = P_u + d_{max}$. Figure 10 shows this theory in more detail and introduces the concept of total depth of metal penetration, which is essentially the correlation and approximate contribution of the average thickness loss determined from LPR corrosion measurements in addition to the pit depth relative to the corroding surface from profilometry measurements. The notion of the total pit penetration depth or metal penetration is effectively what should be used to determine a *total pit penetration rate* which can then be used to estimate pipeline lifetime. Referring to Figure 10, the change in total penetration depth (i.e. uniform thickness plus pit depth relative to the corroded surface) as a function of time can be observed for each solution pH.

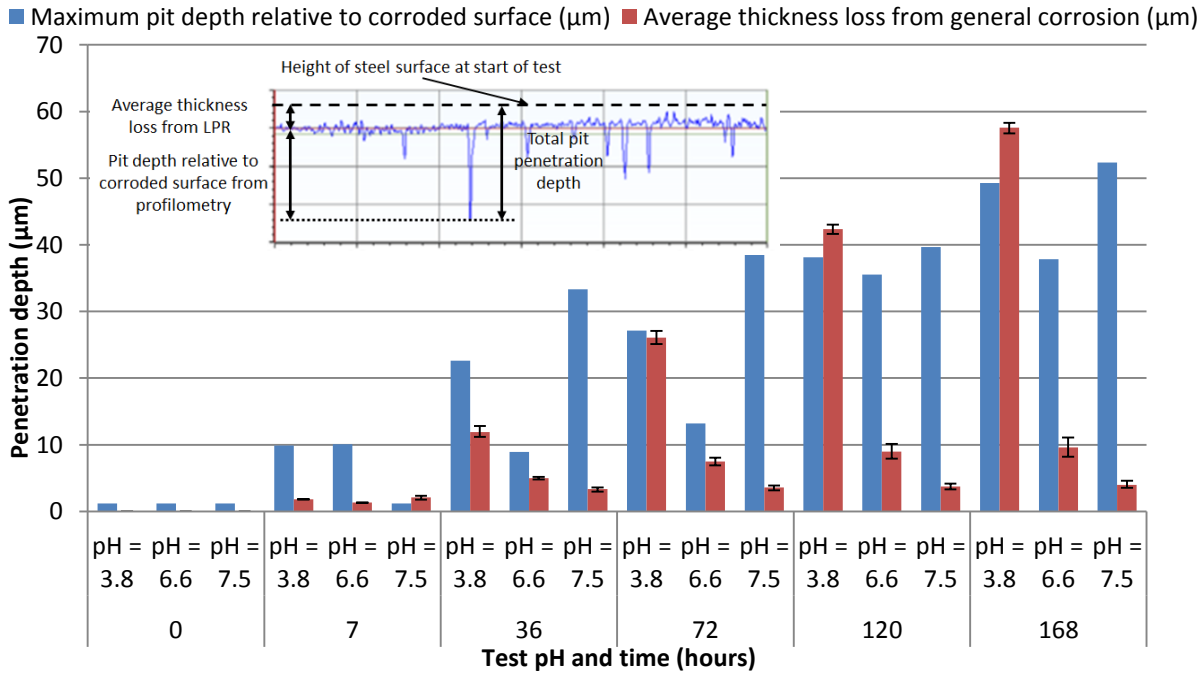

Figure 10: Total pit penetration on steel surface for each system pH as a fuunction of time indicating the contribution of general thickness loss (from LPR) and pit depth relative to corroded surface (determined from surface profilometry)

The results indicate that due to the substantial general corrosion rate of the sample exposed to the pH 3.8 solution, the total penetration depth far exceeds that of the samples exposed to the higher pH solutions, where the uniform thickness loss is negligible in comaprison to the pit depth. It could be considered that the high general corrosion rate observed at pH 3.8 has the ability to essentially mask pit growth. It is therefore logical to conclude that metal penetration is occuring at a faster rate than that identified from purely the profilometry depth measurements relative to the corroding surface.

Therefore affording consideration to the uniform corrosion rate of the surrounding area is a fundamental consideration when reviewing the susceptibility of the carbon steel to pitting corrosion when the general corrosion rate is appreciable. For tests performed at pH 6.6 and 7.5, the growth of the pit is not significantly masked by the general corrosion rate. The results shown in Figure 10 also suggest that in these particular tests, increasing solution pH may not necessarily reduce the risk of pitting of carbon steel materials.

In order to emphasize the importance of this approach, Figure 11 presents a comparison between corrosion rate from experiments in this work at pH of 3.8 and 6.6 with those from the NORSOK standard M-506 open model. For the application of the model in the case of experiments at pH 3.8 (unbuffered), the average pH for the whole duration of the test was used and was ≈ 4.8. The results in Figure 11 shows that the NORSOK standard M-506 model predicted a higher thickness loss due to uniform corrosion than from experiment at starting pH values of 3.8, while on the other hand, the NORSOK standard M-506 model predicted a similar thickness loss due to uniform corrosion at pH 6.6 with estimated thickness loss from experiments. The results in Figure 11 indicate that (in comparison to the pitting and uniform corrosion data provided in Figure 10) although the NORSOK standard M-506 model may not have been developed to predict pitting corrosion, prediction of thickness loss of pipeline steels based on this model in conditions where pitting is likely to occur may be underestimated especially at higher pH values given the strong sensitivity of this model to pH.

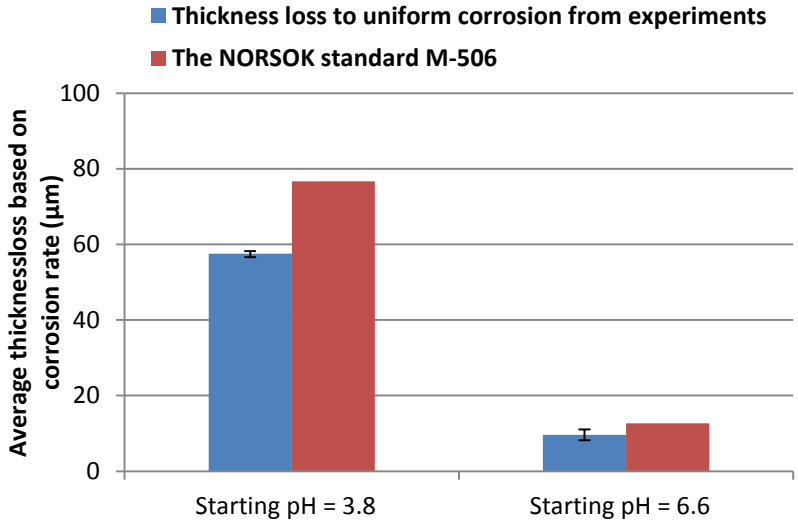

Figure 11: Comparison between the thickness loss due to unform corrosion from experiment and those predicted using the NORSOK standard M-506 model

Pitting Factor: The concept of pitting factor(P_f) has been introduced as a tool for characterization of the nature of corrosion damage in this work. The pitting factor is used to reflect the relative contribution of corrosion damage mechanism (between uniform and pitting corrosion) at each experimental sampling time and is defined in ASTM G46-94[15] as:

$$P_f = (\frac{P_d}{P_u}) \quad (6)$$

Where P_d is the deepest metal penetration (µm) for the whole exposed surface area (sum of maximum pit depth (d_{max}), (after removal of corrosion products) plus the average metal penetration (µm) from general corrosion rate measurement (termed P_u), i.e; $P_d = P_u + d_{max}$.

The deepest metal penetration is the deepest pit (d_{max}) after removal of corrosion products on an entire sample surface while average metal penetration (P_u) is the average of thickness loss due to uniform corrosion as estimated from four repeatable LPR measurements. Hence, the plot of pitting factor in Figure 12 has already taken into consideration the repeatability and variability in the corrosion rate data presented in Figure 3.

As shown in Equation 6, a pitting factor of 1 represents uniform corrosion. The greater the (d_{max}), the greater the pitting factor.

The pitting factor analysis presented in Figure 12 is a clear indication that the corrosion damage mechanism observed at pH 3.8 conditions is actually pitting even while there is still substantial uniform corrosion taking place. At pH 6.6, the pitting factor was higher after 36 hours once significant protection was achieved from precipitated $FeCO_3$ corrosion products. This suggests that pitting corrosion dominated the corrosion damage mechanism in this situation once the corrosion product become significantly protective. This is likely due to the galvanic action that exists [24] between protected and unprotected areas of the corroding surface. The pitting factor at pH of 7.5 was higher after just 7 hours. Thus, at pH 7.5 there was very minimal uniform corrosion.

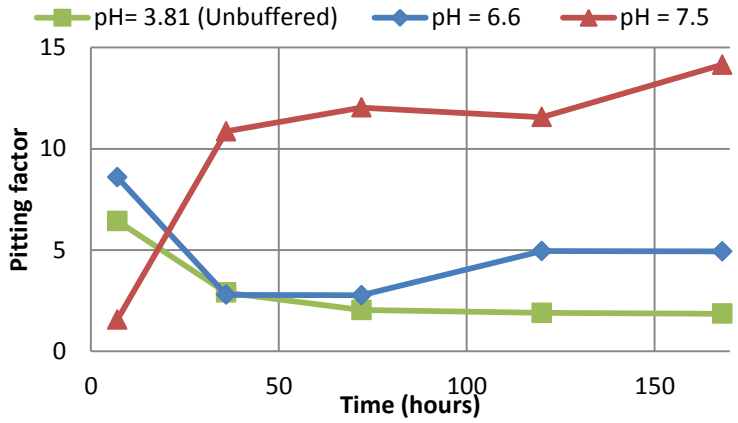

Figure 12: Variation of pitting factor for steel surface exposed to each system pH as a function of time.

Pit count and morphology: Figure 13 provides examples of pit morphologies for the tests conducted at each solution pH. Although no quantative pit count was conducted, the number of pits on the surface were observed to significantly reduce with an increase in solution pH.

At pH 7.5, only 4-5 pits above a depth of 10 µm were observed on the entire steel surface. The difficulty in locating pits under these conditions highlights the importance of ensuring that the entire steel surface is scanned in order to accurately determine the susceptibility of the surface to pitting corrosion, particularly at high pH when the steel enters a pseudo-passive regime.

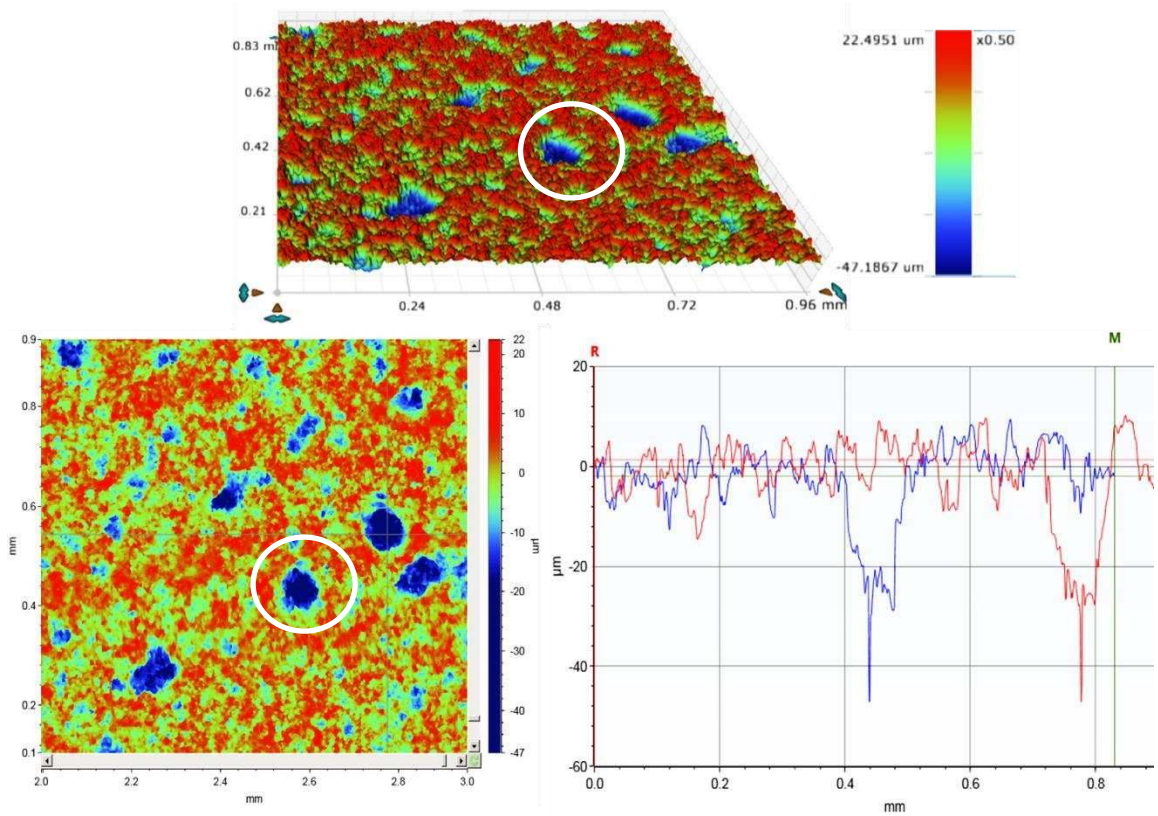

(a) At a starting pH of 3.8 (unbuffered)

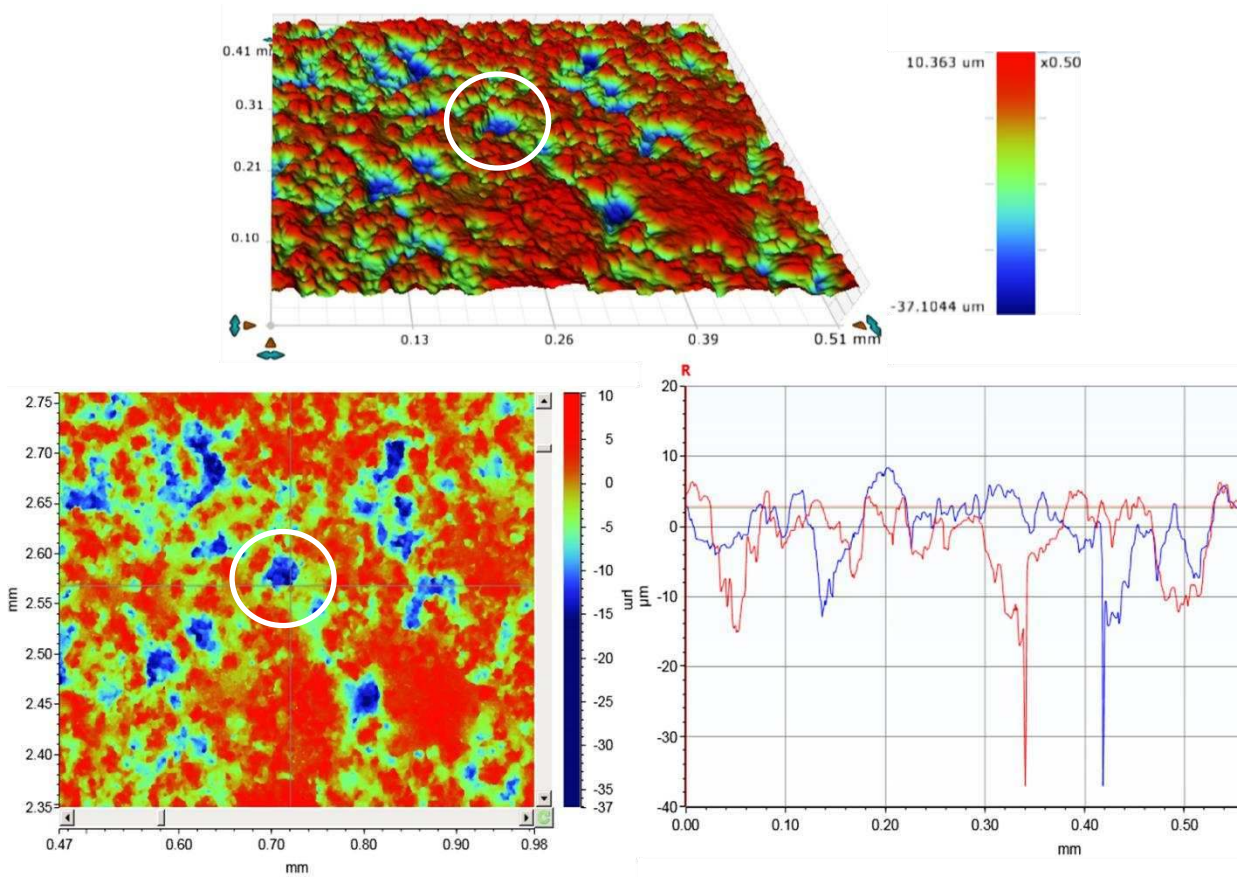

(b) At pH of 6.6 (buffered)

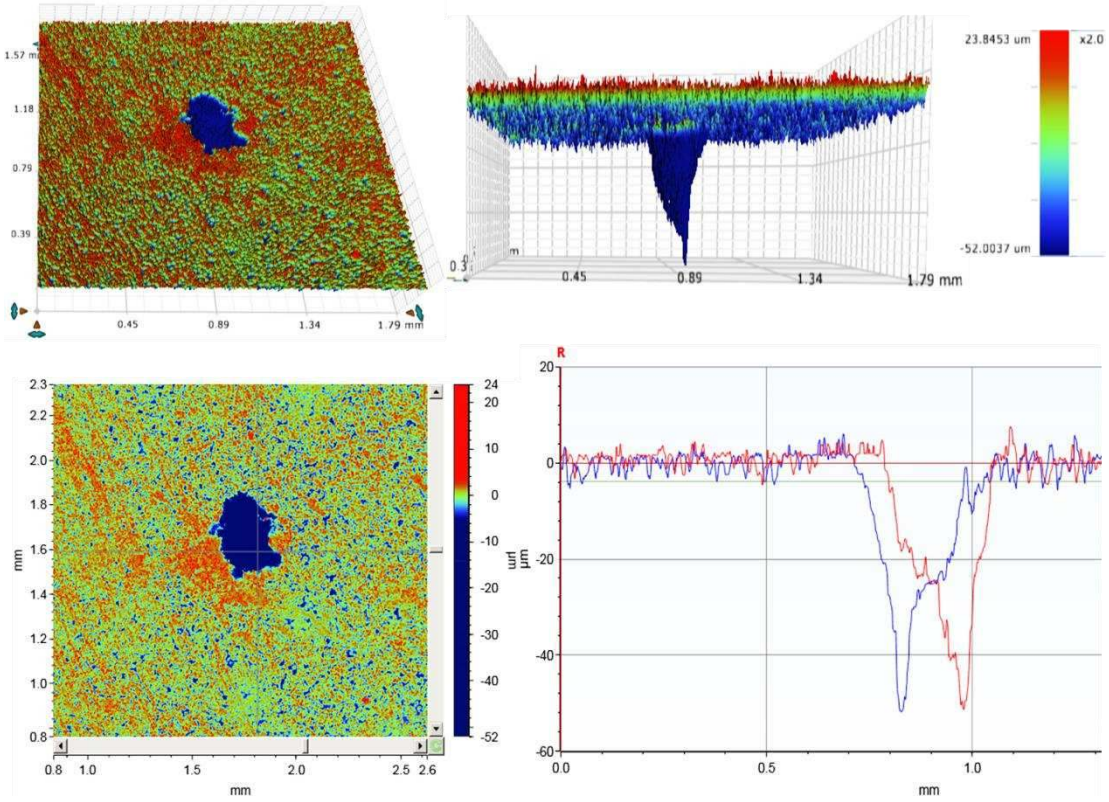

(c) At pH of 7.5 (buffered)

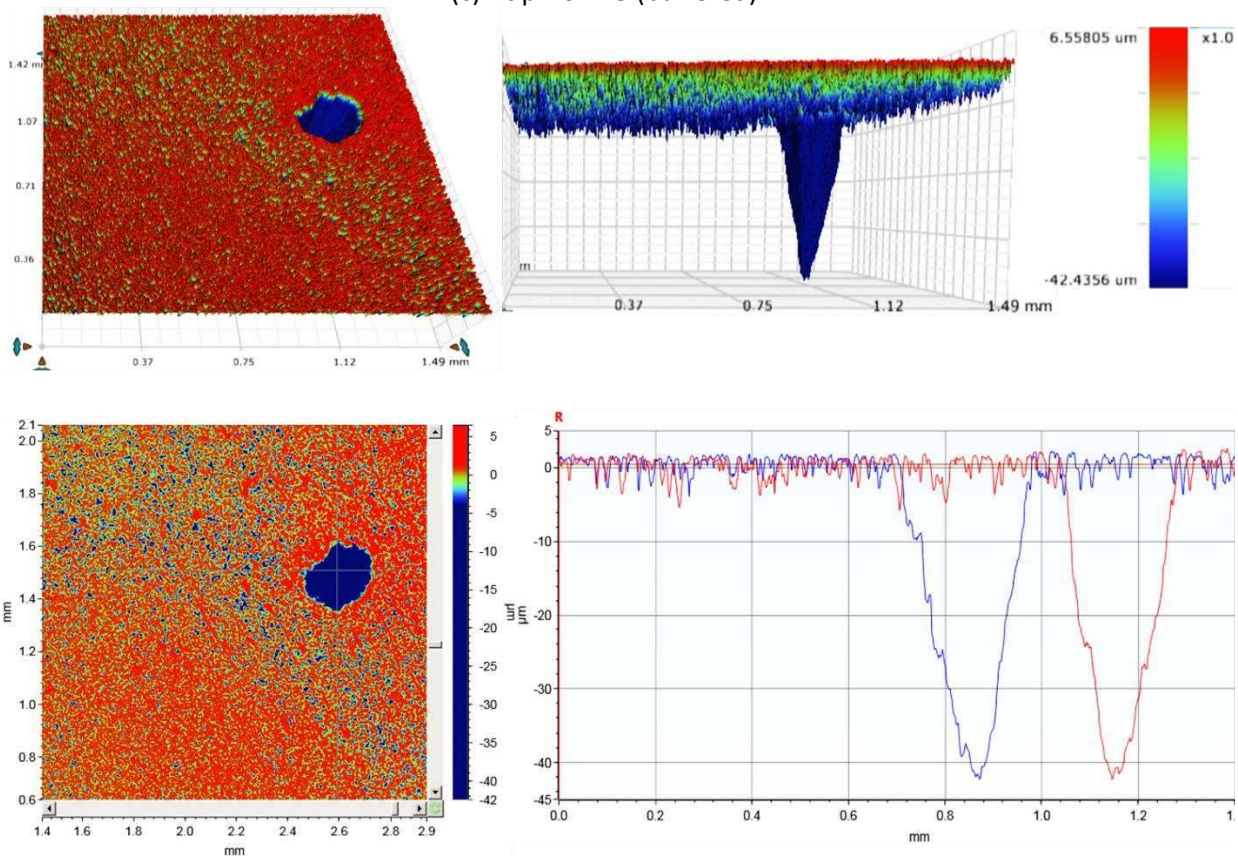

(d) At pH of 7.5 (buffered)

Figure 13: 2D and 3D profilometry images to indicate the morphology and quantity of pits observed on the steel surface after 168 hours exposure to CO_2-saturated brine at a pH of (a) 3.8, (b) 6.6 (c) 7.5 from test-1 and (d) 7.5 from test-2

Influence of pseudo-passivation on pit initiation and propagation

The formation of a passivating oxide layer in passive materials is fundamental to the occurence of pit initiation and propagation. However, similar circumstances have been shown in this work at pH of 7.5 where a pseudo-passivating effect is obserevd on carbon steels. A pseudo-passivated steel surface can therefore act as a large cathode relative to the small anodic pits. However, if already initiated pits are covered by precipitated $FeCO_3$ corrosion products, pit propagation is likely to be inhibited [24].

Figure 10 indicates the change in pit depth as a function of time. By considering the change in total penetration depth (the sum of maximum pit depth relative to corroded surface and the average of thickness loss due to uniform corrosion from four repeatable measurements) between each measurement along with the time interval between the removal of each sample, it is possible to determine the total pit penetration *rate* as a function of time. This information has been extracted from Figure 10 and the pit penetration rate as a function of time but limited to a 168 hours time frame is provided in Figure 14 in conjunction with the OCP measurements for pH 7.5 also as a function of time. The results confirm the previous statement that pit growth is exceptionally high (in excess of 10 mm/year) during the pseudo-passivation process, but after passivation is complete and the potential stabilizes, the pit growth is reduced dramatically to ≈ 0.06 mm/.

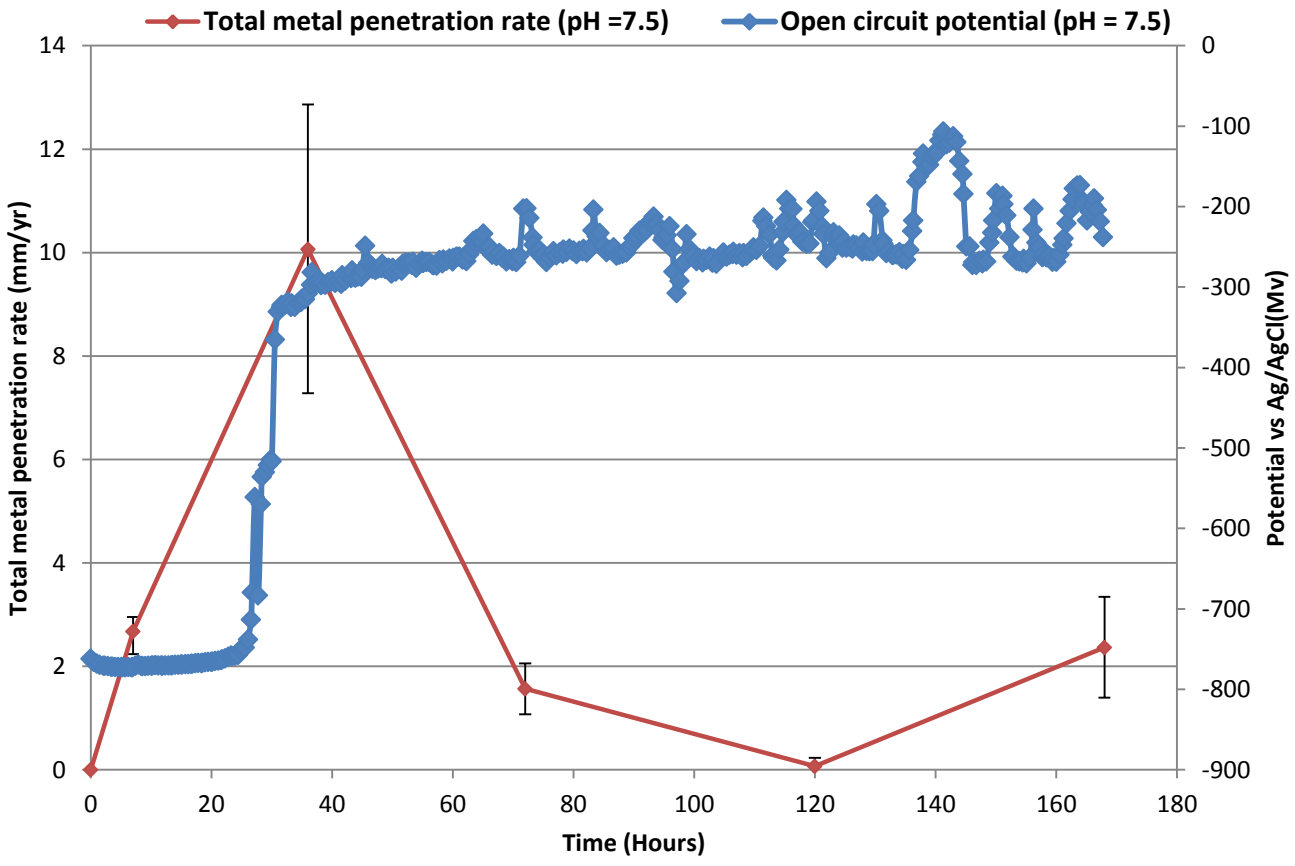

Figure 14: Total metal penetration rate and open circuit potential for X65 steel at pH 7.5 as a function of time. (Error bars are based on variability in pit depth and corosion rate measurements)

CONCLUSIONS

Three different combinations of corrosion products were produced on the surface of X65 carbon steel in 3.5 wt. % NaCl at 50°C and different pH values at 3.8, 6.6 and 7.5. At a starting pH of 3.8 (unbuffered), a non-protective porous Fe_3C film was produced with traces of an amorphous-like product (determined to be $FeCO_3$). At pH 6.6, a protective iron carbonate film was produced and at pH 7.5, an iron carbonate film was formed with a pseudo-passivating effect. From the work performed, the following conclusions can be made. Over a 168 hours exposure period,

- Changing bulk pH influences the kinetics of corrosion and formation of different forms of $FeCO_3$ corrosion product by;
    - Influencing the uniform corrosion rate of steel surface such that the general corrosion rate is reduced with decrease in H+ concentration as the bulk pH increases.
    - Controlling the process of evolution of different forms of $FeCO_3$ corrosion products as the pH changes.
- A correlation between the evolution of different forms of corrosion products at different bulk pH and pitting corrosion has also been established from this study in terms of the pitting corrosion pathways;
- At pH 3.8 (unbuffered), pitting corrosion (relative to corroded surface) occurs steadily.
- At pH 6.6 pitting corrosion also progresses substantially with $FeCO_3$ formation.
- At pH 7.5 pitting corrosion still occurs once pseudo-passivation effect is achieved

REFERENCES

1. R. Nyborg. "Overview of CO_2 corrosion models for wells and pipelines", CORROSION paper no. 2233, (Denver, CO.: NACE International, Houston, Texas, 2002).
2. A. Dugstad. "Fundamental Aspects of CO_2 Metal Loss Corrosion - Part 1: Mechanism", CORROSION paper no. 06111, (San Diego, CA.: NACE International, Houston, Texas, 2006).
3. R. Barker, X. Hu, A. Neville, and S. Cushnaghan, "Empirical Prediction of Carbon-Steel Degradation Rates on an Offshore Oil and Gas Facility: Predicting CO_2 Erosion-Corrosion Pipeline Failures Before They Occur", Society of Petroleum Engineers Journal, (2013).
4. S. Nesic, J. Postlethwaite, and S. Olsen, "An electrochemical model for prediction of corrosion of mild steel in aqueous carbon dioxide solutions", Corrosion, 52, 04 (1996): p. 280-294.
5. Y. Hua, R. Barker, T. Charpentier, M. Ward, and A. Neville, "Relating iron carbonate morphology to corrosion characteristics for water-saturated supercritical CO_2 systems", The Journal of Supercritical Fluids, 98, 0 (2015): p. 183-193.
6. W. Li, B. Brown, D. Young, and S. Nešić, "Investigation of pseudo-passivation of mild steel in CO_2 corrosion", Corrosion, 70, 3 (2013): p. 294-302.

7. J. Han, Y. Yang, S. Nesic, and B.N. Brown. "Roles of passivation and galvanic effects in localized CO_2 corrosion of mild steel", CORROSION, paper no. 332, (New Orleans, LA: NACE International, 2008).

8. R. Nyborg, *Controlling internal corrosion in oil and gas pipelines*, 2005: BUSINESS BRIEFING: EXPLORATION & PRODUCTION: THE OIL & GAS REVIEW 2005.

9. A. Dugstad, L. Lunde, and S. Nesic. "Control of internal corrosion in multi-phase oil and gas pipelines", Prevention of pipeline corrosion conference, (Houston, TX, 1994).

10. F. Farelas, Y.S. Choi, and S. Nešić, "Corrosion Behavior of API 5L X65 Carbon Steel under Supercritical and Liquid Carbon Dioxide Phases in the Presence of Water and Sulfur Dioxide", Corrosion, 69, 3 (2012): p. 243-250.

11. F. Farelas, M. Galicia, B. Brown, S. Nesic, and H. Castaneda, "Evolution of dissolution processes at the interface of carbon steel corroding in a CO_2 environment studied by EIS", Corrosion Science, 52, 2 (2010): p. 509-517.

12. J. Crolet, N. Thevenot, and S. Nesic, "Role of Conductive Corrosion Products in the Protectiveness of Corrosion Layers", Corrosion, 54, 3 (1998): p. 194-203.

13. B.M. Kermani and A. Morshed, "Carbon dioxide corrosion in oil and gas production: A compendium", Corrosion, 59, 08 (2003): p. 659-683.

14. A. Dugstad. "Mechanism of protective film formation during CO_2 corrosion of carbon steel", CORROSION, paper no.31, (San Diego, CA: NACE International, Houston, Texas, 1998).

15. ASTM Standard G46-94, Standard guide for examination and evaluation of pitting corrosion. ASTM International: West Conshohocken, PA, 2003.

16. Y. Zheng, J. Ning, B. Brown, and S. Nešić, "Electrochemical Model of Mild Steel Corrosion in a Mixed H_2S/CO_2 Aqueous Environment in the Absence of Protective Corrosion Product Layers", Corrosion, 71, 3 (2015): p. 316-325.

17. Y. Hua, R. Barker, and A. Neville, "Comparison of corrosion behaviour for X-65 carbon steel in supercritical CO_2-saturated water and water-saturated/unsaturated supercritical CO_2", The Journal of Supercritical Fluids, 97, 0 (2015): p. 224-237.

18. F. Pessu, R. Barker, and A. Neville. "Understanding pitting corrosion behaviour of X-65 (UNS K03014) carbon steel in CO_2 saturated environments: The temperature effect", CORROSION, paper no. 4214, (San Antonio, TX: NACE International, Houston, Texas, 2014).

19. S. Guo, L. Xu, L. Zhang, W. Chang, and M. Lu, "Corrosion of alloy steels containing 2% chromium in CO_2 environments", Corrosion Science, 63, (2012): p. 246-258.

20. J. Han, D. Young, H. Colijn, A. Tripathi, and S. Nešić, "Chemistry and Structure of the Passive Film on Mild Steel in CO_2 Corrosion Environments", Industrial & Engineering Chemistry Research, 48, 13 (2009): p. 6296-6302.

21. I.G. Wood, L. Vocadlo, K.S. Knight, D.P. Dobson, W.G. Marshall, and G.D.B. Price, J., "Thermal expansion and crystal structure of cementite, Fe_3C, between 4 and 600 K determined by time-of-flight neutron powder diffraction Note:T=540 K", Journal of Applied Crystallography, 37, (2004): p. 9.

22. K.M. H. Effenberger, and J. Zemann, "Crystal structure refinements of magnesite, calcite, rhodochrosite, siderite, smithonite, and dolomite, with discussion of some aspects of the stereochemistry of calcite type carbonates", Z. Kristallogr, 156, (1981): p. 11.

23. F. Deganello, L.F. Liotta, A. Longo, M.P. Casaletto, and M. Scopelliti, "Cerium effect on the phase structure, phase stability and redox properties of Ce-doped strontium ferrates", Journal of Solid State Chemistry, 179, 11 (2006): p. 3406-3419.

24. J. Han, B.N. Brown, and S. Nešić, "Investigation of the galvanic mechanism for localized carbon dioxide corrosion propagation using the artificial pit technique", Corrosion, 66, 9 (2010): p. 12.